GEOPHYSICS, VOL. 76, NO. 3 (MAY-JUNE 2011); P. WA43–WA50, 5 FIGS., 1 TABLE.
10.1190/1.3555530

A comparison of the dispersion relations for anisotropic elastodynamic finite-difference grids

Henrik Bernth[1] and Chris Chapman[1]

ABSTRACT

Several staggered grid schemes have been suggested for performing finite-difference calculations for the elastic wave equations. In this paper, the dispersion relationships and related computational requirements for the Lebedev and rotated staggered grids for anisotropic, elastic, finite-difference calculations in smooth models are analyzed and compared. These grids are related to a popular staggered grid for the isotropic problem, the Virieux grid. The Lebedev grid decomposes into Virieux grids, two in two dimensions and four in three dimensions, which decouple in isotropic media. Therefore the Lebedev scheme will have twice or four times the computational requirements, memory, and CPU as the Virieux grid but can be used with general anisotropy. In two dimensions, the rotated staggered grid is exactly equivalent to the Lebedev grid, but in three dimensions it is fundamentally different. The numerical dispersion in finite-difference grids depends on the direction of propagation and the grid type and parameters. A joint numerical dispersion relation for the two grids types in the isotropic case is derived. In order to compare the computational requirements for the two grid types, the dispersion, averaged over propagation direction and medium velocity are calculated. Setting the parameters so the average dispersion is equal for the two grids, the computational requirements of the two grid types are compared. In three dimensions, the rotated staggered grid requires at least 20% more memory for the field data and at least twice as many number of floating point operations and memory accesses, so the Lebedev grid is more efficient and is to be preferred.

INTRODUCTION

In exploration seismology, finite-difference modeling has in the past been used mainly as a tool for generating synthetic datasets and for survey design. With the emergence of acoustic reverse-time migration and full waveform inversion as practical data processing options, finite-difference modeling now plays an even more prominent role. The improvements in the performance of software and hardware mean that anisotropic, full wave-equation modeling, migration, and even inversion are becoming realistic prospects. Nevertheless the required 3D, general anisotropic modeling is still a challenge. Finite-difference schemes to solve the elastic wave equation are popular but suffer from several numerical problems. Several schemes have been suggested for finite-difference calculations, and it is important to investigate their properties in order to make an optimum choice. Numerical errors in finite-difference calculations can occur due to numerical dispersion (waves traveling with a frequency-dependent velocity due to the discrete grid), stability (errors growing exponentially), reflections from the edge of the model (inefficient absorbing boundary conditions), and inaccurate boundary conditions (at the free surface and boundaries within the model). The cost of a 3D finite-difference simulation is roughly proportional to $1/h^4$, where h is the grid spacing, because the number of grid cells is proportional to $1/h^3$ and the number of time steps to $1/h$. Resolution of model detail may dictate a fine grid spacing, but for smooth models the grid spacing is largely determined by the need to control numerical dispersion. For an overview of finite-difference modeling, see Moczo et al. (2007).

In this paper we compare and relate two proposed grids — the Lebedev and rotated staggered grids — and draw important conclusions for the optimal choice based on the computational requirements to obtain the same average numerical dispersion. This has implications for applications such as reverse-time migration and full waveform inversion. In this paper, we restrict the discussion to the dispersion results and do not discuss issues such as boundary conditions that may differ between grids.

Manuscript received by the Editor 4 August 2010; revised manuscript received 26 October 2010; published online 23 May 2011.
[1]Schlumberger Cambridge Research, Cambridge, England. E-mail: bernth@cambridge.oilfield.slb.com; chapman@cambridge.oilfield.slb.com.

For isotropic models, a scheme such as Virieux's staggered grid (Virieux, 1986), with the velocity-stress formulation of the elastic wave equation, works well and minimizes memory and compute time requirements. However, the scheme breaks down for anisotropic models, although it can be repaired by interpolating the derivatives of certain field variables at the grid cell locations where they are needed (Igel et al., 1995). In this paper, we analyze and compare the computational requirements and dispersion properties for two schemes that handle the anisotropic problem without interpolation: the Lebedev grid (Lebedev, 1964; Lisitsa, 2007) and the rotated staggered grid (Saenger et al., 2000). This comparison is crucial for the correct choice of the optimal method. Throughout the paper we use the suffices LEB and ROT to indicate variables in these schemes.

Lisitsa and Vishnevskiy (2010) have made a similar comparison. Their discussion is restricted to the second-order method without averaging over direction. For an elaborate cost-based comparison of finite-difference schemes for the acoustic wave equation see Anné et al. (1997).

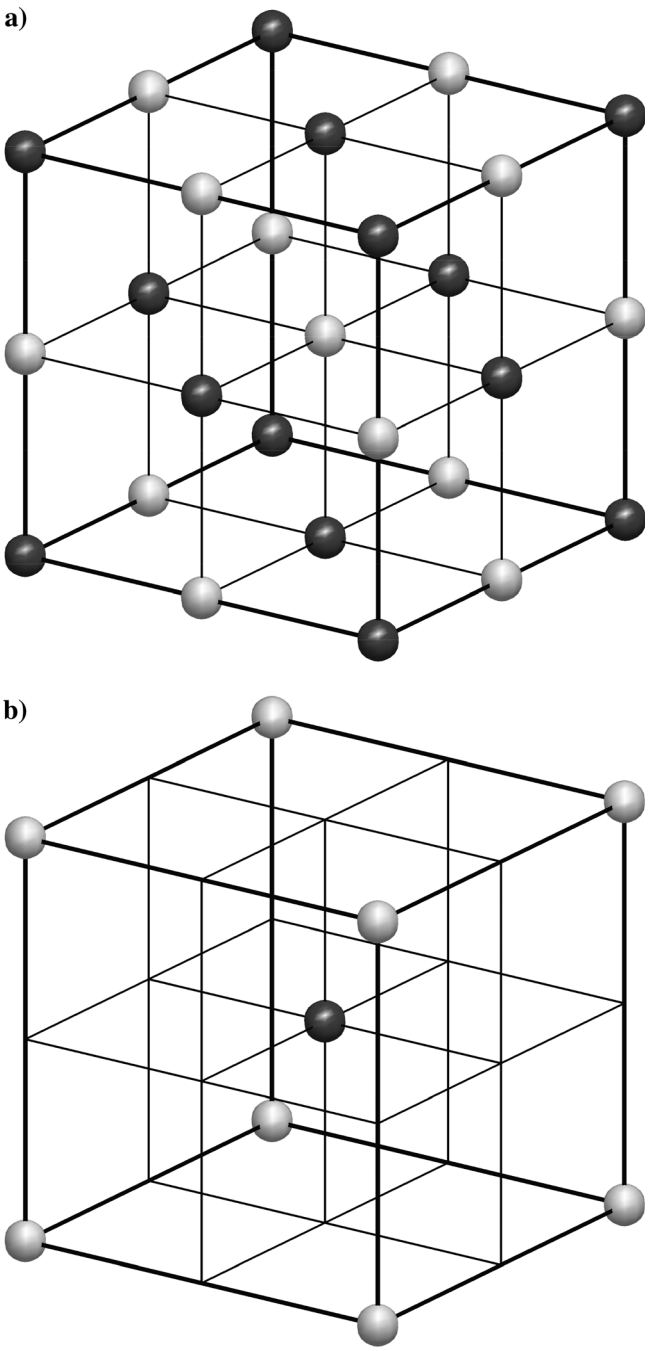

Figure 1. The (a) 3D Lebedev and (b) rotated staggered grid cell. The particle velocity, $\mathbf{v}$, is stored at the light grid points and the stress, $\boldsymbol{\sigma}$, at the dark grid points.

THE LEBEDEV AND THE ROTATED STAGGERED GRID

We define a 3D grid with grid cell corners located at

$$\mathbf{x} = \mathbf{x}_{ijk} = \mathbf{x}_{000} + h(i\hat{\mathbf{e}}_1 + j\hat{\mathbf{e}}_2 + k\hat{\mathbf{e}}_3), \tag{1}$$

where for simplicity we assume the cell is a cube, and $\hat{\mathbf{e}}_i$ are the unit cartesian basis vectors. The seven staggered subgrids are defined at the edge, face, and cell mid-points, e.g., $\mathbf{x}_{i+1/2jk}, \ldots, \mathbf{x}_{ij+1/2k+1/2}, \ldots, \mathbf{x}_{i+1/2j+1/2k+1/2}$, making eight subgrids in all.

In the 3D Lebedev staggered grid, the full stress and full velocity are stored on alternating points. Thus, as shown in Figure 1a,

- the stress $\boldsymbol{\sigma}$, is stored at $\mathbf{x}_{ijk}$, $\mathbf{x}_{ij+1/2k+1/2}$, $\mathbf{x}_{i+1/2jk+1/2}$ and $\mathbf{x}_{i+1/2j+1/2k}$;
- the particle velocity $\mathbf{v}$, is stored at $\mathbf{x}_{i+1/2jk}$, $\mathbf{x}_{ij+1/2k}$, $\mathbf{x}_{ijk+1/2}$ and $\mathbf{x}_{i+1/2j+1/2k+1/2}$,

i.e., the stress and particle velocity are stored on four subgrids each. Spatial derivatives are approximated by difference operators acting in the directions of the coordinate axes, and the derivatives required for general anisotropy can be calculated without interpolation because there's always a stress node between two velocity nodes and vice versa. Each grid cell requires storage of 36 field variables, and there are $36/(h^{\mathrm{LEB}})^3$ field variables per unit volume. In the Virieux grid, only some components of stress and velocity are stored at each subgrid point, and each grid cell only stores nine field variables.

The rotated staggered grid cell stores velocities at each corner and stress at the center of the cell. Thus in Figure 1b,

- $\boldsymbol{\sigma}$ is stored at $\mathbf{x}_{i+1/2j+1/2k+1/2}$;
- $\mathbf{v}$ is stored at $\mathbf{x}_{ijk}$.

Only the corner and cell mid-point subgrids are used. Derivatives are calculated on diagonals and rotated to the coordinate axes. In the formulae for the coordinate derivatives, all diagonal derivatives contribute through sums and differences [see, e.g., the formulae 16 to 18 in Saenger et al. (2000)]. Each grid cell requires storage of nine field variables, and there are $9/(h^{\mathrm{ROT}})^3$ field variables per unit volume.

First we briefly review the dispersion results in two dimensions, which are simpler than those in three dimensions. It is straightforward to see that the Lebedev grid is equivalent to two Virieux grids, one shifted so the cell corner is at the center of the other's cell. In two dimensions, the rotated staggered grid is *exactly* equivalent to a rotated Lebedev grid — hence the name — with smaller cell size $h^{\mathrm{ROT}} = h^{\mathrm{LEB}}/\sqrt{2}$ (see Figure 2). However, in three dimensions, the rotated staggered grid is fundamentally different (the cell in Figure 1b has four diagonals

through the central subgrid point, and so it is impossible to rotate these into three axes).

DISPERSION RELATIONS

We consider the velocity-stress formulation of the elastic wave equation

$$\rho \partial_t v_i = \partial_j \sigma_{ij} \tag{2}$$

$$\partial_t \sigma_{ij} = c_{ijk\ell} \partial_\ell v_k, \tag{3}$$

using the Einstein summation notation. In order to compare the LEB and ROT grids, we first derive the dispersion relations for these grids (details on the derivations are given in Appendix A). Using these relations, we compare the results for the two schemes and determine the relative cell sizes that give the same average dispersion (averaged over direction and over media velocity) for the two grids.

The dispersion results are derived for the homogeneous isotropic case. They are based on a standard von Neumann analysis with a trial plane-wave solution

$$u(t, \mathbf{x}) = \mathrm{e}^{\mathrm{i}(\omega t - \mathbf{k}\cdot\mathbf{x})}, \tag{4}$$

where ω is the circular frequency and $\mathbf{k}$ is the wave vector. LEB and ROT use the same temporal difference operator given by

$$D_T u(t, \mathbf{x}) = \frac{1}{\Delta t}(u(t + \Delta t/2, \mathbf{x}) - u(t - \Delta t/2, \mathbf{x})), \tag{5}$$

where Δt is the time step. The spatial operators are of the form

$$D_S(\mathbf{b})u(t, \mathbf{x}) = \sum_{m=1}^{M} c_{mM}(u(t, \mathbf{x} + (2m-1)\mathbf{b}) - u(t, \mathbf{x} - (2m-1)\mathbf{b})), \tag{6}$$

for an operator of length $(2M)$. Here $\mathbf{b}$ is a vector that for LEB schemes is parallel to one of the coordinate axes, i.e., $\mathbf{b} = h\hat{\mathbf{e}}/2$, where $\hat{\mathbf{e}}$ is a Cartesian basis vector and for ROT schemes is parallel to one of the diagonals, i.e., $\mathbf{b} = h\sqrt{N}\hat{\mathbf{d}}/2$, where $N = 2$ or 3, the grid dimension and $\hat{\mathbf{d}}$ is a diagonal unit vector. The constants c_{mM} are conventionally determined to achieve the highest possible order $(2M)$ in the operator, i.e., using the exact Taylor expansion, and we shall refer to such operators as *standard operators*. However, they may also be designed to optimize other measures of accuracy (Holberg, 1987). Many authors have published tables of the standard operator coefficients c_{mM} for the commonly used low orders, and Fornberg (1990) has derived a simple recursive formula that can be used for any order. The low-order values are given in Table 1.

Following the normal practice (Virieux, 1986), we shall write the dispersion relations in terms of two dimensionless numbers

$$\gamma = \frac{v\Delta t}{h} \tag{7}$$

$$H = \frac{kh}{2\pi} = \frac{\omega h}{2\pi c}, \tag{8}$$

where $k = |\mathbf{k}|$ is the wavenumber, and $c = \omega/k$ is the phase velocity (see equation 4). The first, γ, is known as the Courant number and must be less than a certain constant $\gamma_{\max}$ for the scheme to be stable. The maximum value for this number for

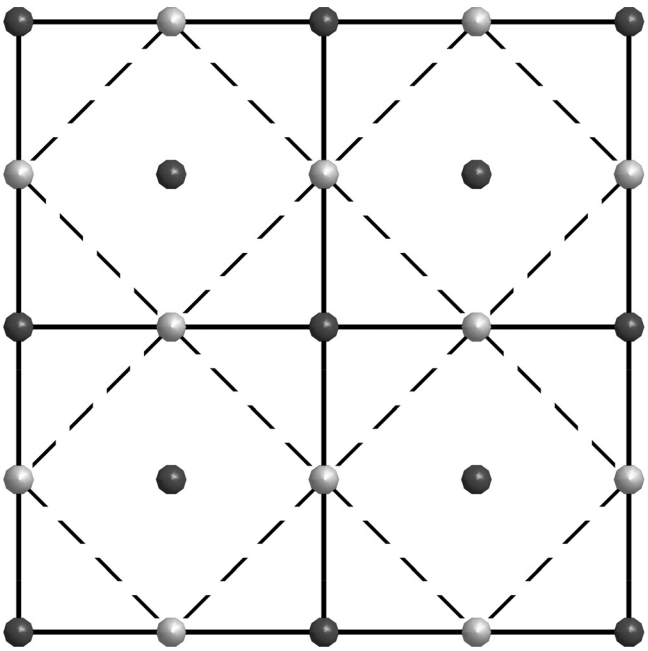

Figure 2. The 2D rotated staggered grid cell (dashed line) superimposed on a two dimensional Lebedev grid (solid line).

Table 1. The coefficients, c_{mM}, for the second- to eighth-order, finite-difference operators, equation 6, and the corresponding 2D and 3D Courant numbers, equation 9.

	c_{mM}				$\sum_{m=1}^{M} \lvert c_{mM} \rvert$	$\gamma_{\max}^{(2)\,LEB}$	$\gamma_{\max}^{(3)\,LEB}$
M	1st order	2nd order	3rd order	4th order			
1	1				1	0.707	0.577
2	$\frac{9}{8}$	$-\frac{1}{24}$			$\frac{7}{6}$	0.606	0.495
3	$\frac{75}{64}$	$-\frac{25}{384}$	$\frac{3}{640}$		$\frac{149}{120}$	0.569	0.465
4	$\frac{1225}{1024}$	$-\frac{245}{3072}$	$\frac{49}{5120}$	$-\frac{5}{7168}$	$\frac{69157}{53760}$	0.550	0.499

stability in staggered grids is (Saenger et al., 2000, equations 29 and 30)

$$\gamma_{\max}^{(N)\mathrm{LEB}} = \frac{1}{\sqrt{N}\sum_{m=1}^{M}|c_{mM}|}, \tag{9}$$

and

$$\gamma_{\max}^{(N)\mathrm{ROT}} = \sqrt{N}\gamma_{\max}^{(N)\mathrm{LEB}}, \tag{10}$$

where c_{mM} are the constants used in the spatial difference operators (see equation 6). Table 1 lists the maximum Courant numbers for a few low-order operators.

The second number, H, is associated with the error due to dispersion. By Nyquist's theorem, its maximum value is 0.5. Its inverse, H^{-1}, is the number of grid cells per wavelength (in the coordinate directions). The dispersion relation will depend on these two dimensionless numbers, γ and H, and the propagation direction, $\hat{\mathbf{k}} = \mathbf{k}/k = (\hat{k}_x\ \hat{k}_y\ \hat{k}_z)$.

The compact expression we have obtained for the dispersion relation has not appeared in the literature before, but as the algebra is somewhat lengthy, we have relegated it to Appendix A (see Saenger and Bohlen, 2004, for a related result). In terms of the dimensionless parameters, γ and H, expressions 7 and 8, we have derived a single general dispersion relation (equations A-15 and A-21)

$$\frac{c}{v} = \frac{1}{\pi\gamma H}\sin^{-1}\left[\gamma\sqrt{\sum_{n=1}^{N}\left(\sum_{m=1}^{M}c_{mM}\Phi_n\left((2m-1)\pi H\hat{\mathbf{k}}\right)\right)^2}\right], \tag{11}$$

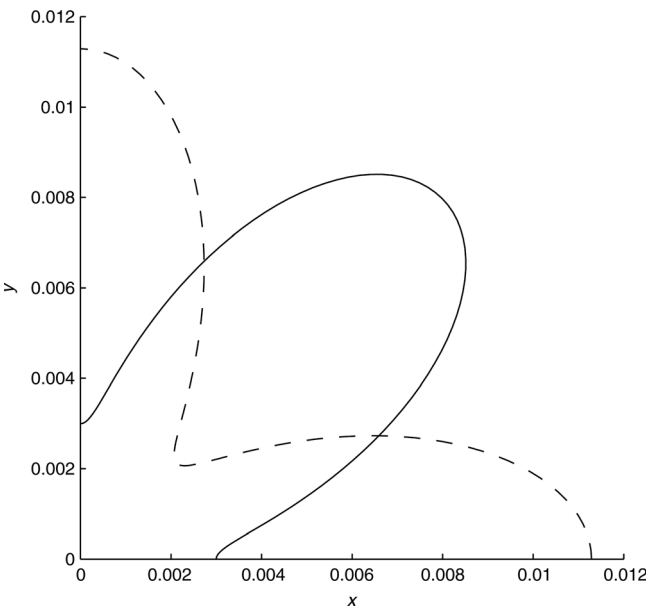

Figure 3. One quadrant of the absolute fractional error in two dimensions from equations 11 and 14, where the solid line is for the ROT scheme, equation 13, and the dashed line is for the LEB scheme, equation 12. The parameters are $\gamma^{\mathrm{ROT}} = v\Delta t/h^{\mathrm{ROT}} = 2^{1/2}\gamma^{\mathrm{LEB}} = 0.8\gamma_{\max}^{(2)\mathrm{ROT}} = 0.8$ and $H^{\mathrm{ROT}} = 2^{-1/2}H^{\mathrm{LEB}} = 0.0707$.

which is valid for the LEB and ROT schemes with alternative functions for Φ_n. The functions Φ_n are defined as

$$\Phi_n^{\mathrm{LEB}}(\mathbf{x}) = \sin(x_n), \tag{12}$$

for the LEB scheme, and

$$\Phi_n^{\mathrm{ROT}}(\mathbf{x}) = \sin(x_n)\cos(x_\ell)\cos(x_m), \tag{13}$$

for the ROT scheme in three dimensions, where l, m, and n are a cyclic permutation of 1, 2, and 3. The LEB dispersion relation, equation 11 with equation 12, also applies to the Virieux scheme.

In order to compare dispersion errors for different schemes, we define a signed fractional error

$$E(\gamma, H, \hat{\mathbf{k}}) = \frac{c}{v} - 1. \tag{14}$$

As well as being a function of the dimensionless numbers, γ and H, equations 7 and 8, and the propagation direction, $\hat{\mathbf{k}}$, the error given by expression 14 depends on the length of the operator, M, and the grid type, LEB or ROT. It is noteworthy that

$$E^{\mathrm{LEB}}(\gamma, H, \hat{\mathbf{d}}) = E^{\mathrm{ROT}}(\gamma\sqrt{N}, H/\sqrt{N}, \hat{\mathbf{e}}), \tag{15}$$

for both two and three dimensions for any spatial operator (note equality is between the error on the diagonal in the LEB grid and the axes in the ROT grid for the same order operator).

DISPERSION IN 2D

First we briefly discuss the result 11 in two dimensions. Figure 3 illustrates the absolute fractional error, i.e., $|E|$ using expression 11, as a function of direction ($\hat{\mathbf{k}}$) for typical values of γ and H, for the Lebedev and rotated staggered grids. Clearly these curves are identical except for a rotation through 45° . We have already commented that the two grids are identical apart from rotation and cell size (Figure 2), so it is expected that the dispersion results will also be identical. It is straightforward to confirm algebraically that expression 11 with expression 12 is the same as expression 11 with expression 13, rotating the unit vector $\hat{\mathbf{k}}$ though 45 , scaling the parameters $\gamma^{\mathrm{ROT}} = 2^{1/2}\gamma^{\mathrm{LEB}}$ and $H^{\mathrm{ROT}} = 2^{-1/2}H^{\mathrm{LEB}}$. The scaling and exact equality of the dispersion relations on the two grids is consistent with equation 15.

DISPERSION IN 3D

In three dimensions the comparison is more complicated as the dispersion errors cannot be made identical. Obviously, grids should be compared when they produce comparable dispersion, not when the grid cells are the same size. We focus on the memory requirements for the field variables as efficient schemes for storing the model parameters are possible (such as look-up tables or compression that avoid storing all the model parameters at every grid point or sharing the model between several simulations progressing in parallel).

The absolute value of the signed fractional error in velocity (expression 12) for the two schemes is illustrated in Figure 4a and b for the second-order ($M = 1$) scheme. For comparison the grid spacings have been chosen so that memory requirements for the schemes are identical. It is obvious that these errors are significantly anisotropic and different, which motivates our more detailed comparison of the *average* error. Fortunately the anisotropy of the dispersion is smaller for higher-order schemes (using

typical parameters). In Figure 5a and b, we have illustrated the errors for the popular fourth-order scheme ($M = 2$).

In a slightly different setting that extends to the LEB scheme, Anné et al. (1997) have shown that for the case of standard differentiators for fixed γ and H, E takes its maximum on a diagonal and its minimum on an axis, noting that the minimum may be the absolute maximum. Numerical studies indicate that for the ROT scheme, E takes its minimum on a diagonal and its maximum on an axis.

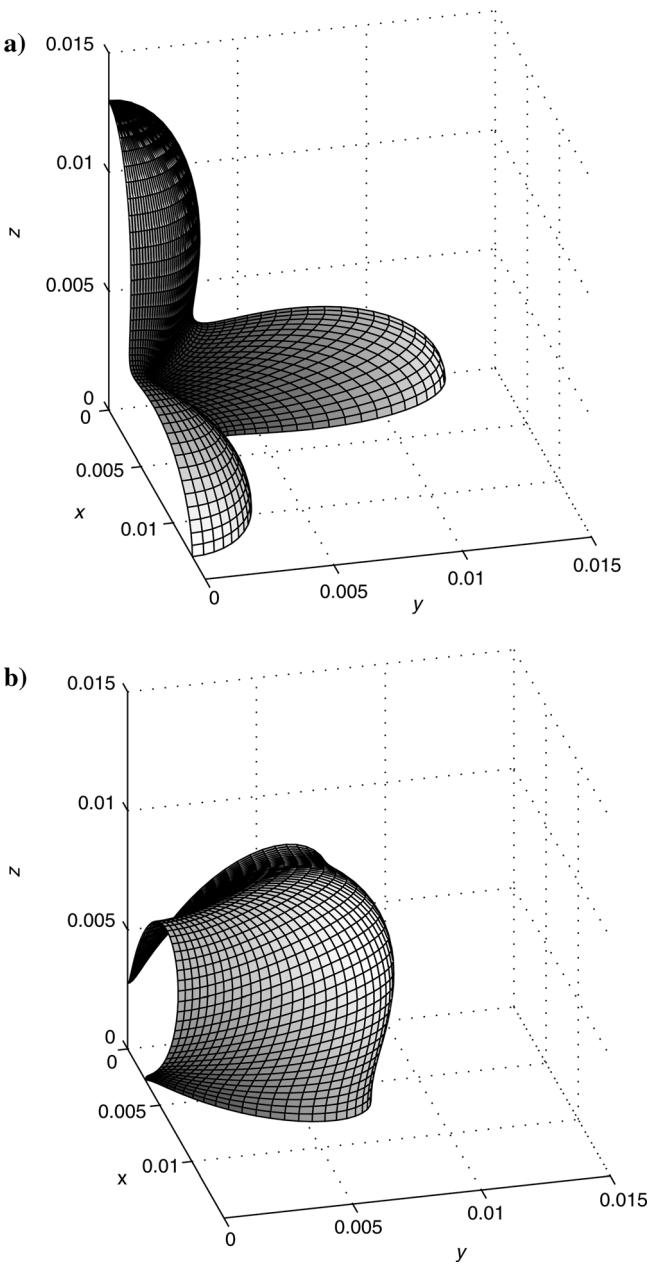

Figure 4. One octant of the absolute fractional error in three dimensions from equations 11 and 14 for (a) the second-order LEB scheme with $\gamma^{\mathrm{LEB}} = 0.8\gamma_{\max}^{(3)\mathrm{LEB}} = 0.462$ and $H^{\mathrm{LEB}} = 0.1$ and for (b) the second-order ROT scheme with $\gamma^{\mathrm{ROT}} = 0.8\gamma_{\max}^{(3)\mathrm{ROT}} = 0.8$ and $H^{\mathrm{ROT}} = 0.068$. The distance from the origin is the absolute error in the corresponding direction. The other octants have reflection symmetry.

We shall not pursue this any further, but rather use the dispersion expressions to evaluate the average of the squared fractional error over all directions. As for spatial operators of order higher than two the fractional error depends less on direction, it is reasonable to consider such an average error. The Courant number,

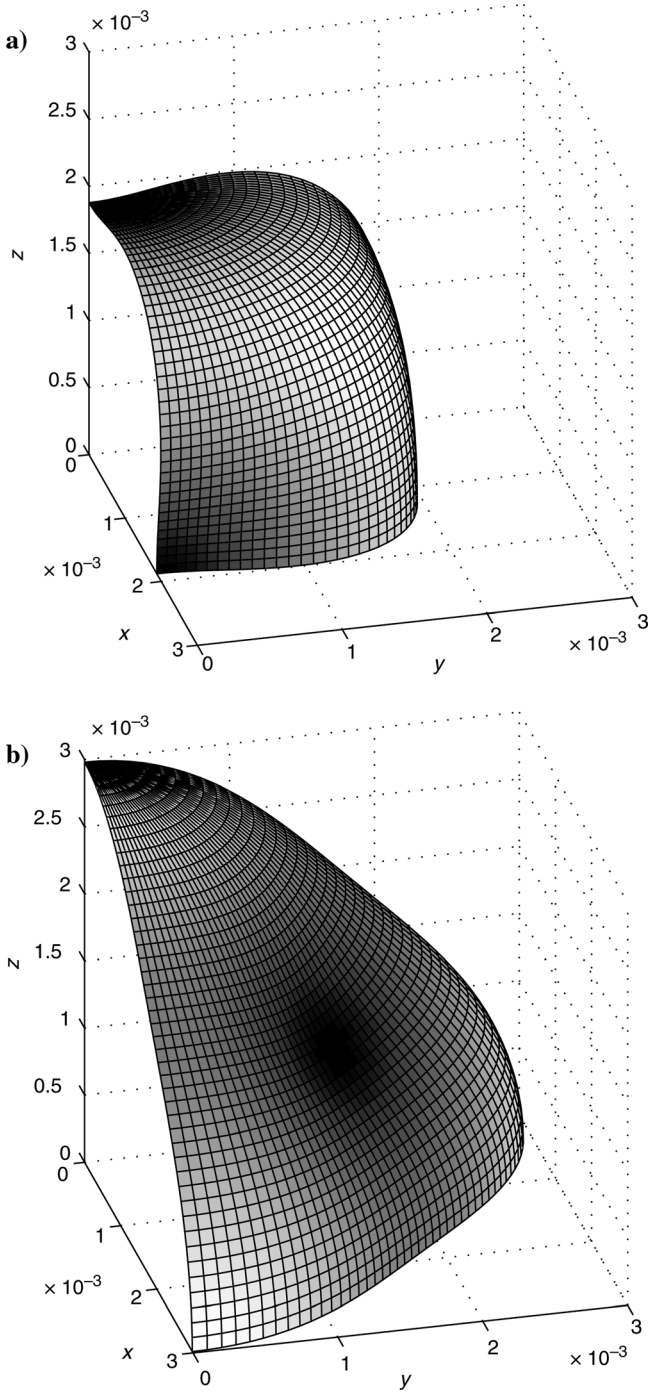

Figure 5. One octant of the absolute fractional error in three dimensions for the standard fourth-order spatial operator. For (a) the LEB scheme $\gamma^{\mathrm{LEB}} = 0.8\gamma_{\max}^{(3)\mathrm{LEB}} = 0.396$ and $H^{\mathrm{LEB}} = 0.1$. For (b) the ROT scheme $\gamma^{\mathrm{ROT}} = 0.8\gamma_{\max}^{(3)\mathrm{ROT}} = 0.686$ and $H^{\mathrm{ROT}} = 0.063$. The distance from the origin is the absolute error in the corresponding direction. The other octants have reflection symmetry.

equation 7, depends on the velocity, which may vary significantly throughout the model. In order to compare the error in a non-model-specific manner, apart from averaging over direction we also need to average over a range of Courant numbers.

We define a normalized Courant number

$$\bar{\gamma} = \gamma/\gamma_{\max}, \tag{16}$$

where $\gamma_{\max}$ is the maximum Courant number. We assume that the velocity in the model varies from $v_{\min}$ to $v_{\max}$, and choose a time step close to the upper limit. Then the normalized Courant number varies between the velocity ratio $r_v = v_{\min}/v_{\max}$ and 1. For a fixed spatial grid spacing, the number of grid points per wavelength increases linearly with the velocity. Thus it seems reasonable to work with a functional relationship between $\bar{\gamma}$ and H of the following kind:

$$H(\bar{\gamma}) = \frac{K}{\bar{\gamma}}, \tag{17}$$

where K is a constant. For a typical model, r_v may have the value 0.25. If we are using the standard fourth-order operator and insist on at least five cells per wavelength, $K = 0.05$.

Combining these parameters, we define an average dispersion error (at a fixed frequency), as

$$\int_{r_v}^{1}\int_{S} E(\bar{\gamma}, K/\bar{\gamma}, \hat{\mathbf{k}})^2 \mathrm{d}S\mathrm{d}\bar{\gamma}, \tag{18}$$

where S is the unit sphere. Unfortunately expression 11 is sufficiently complicated that expression 18 cannot be evaluated analytically, but it is straightforward to compute numerically.

We have evaluated expression 18 for standard operators up to order 10 and for a variety of Holberg-type operators for a range r_v and K values. It turns out that expression 18 takes approximately the same value for the Lebedev and the rotated staggered grid if

$$\frac{K^{\mathrm{LEB}}}{K^{\mathrm{ROT}}} = \frac{H^{\mathrm{LEB}}}{H^{\mathrm{ROT}}} \simeq 1.7. \tag{19}$$

Not surprisingly, this ratio is close to $\sqrt{3}$, the difference between the cell edge and the cell diagonal, the directions used for the spatial operators in the two schemes, i.e., the ratio of the lengths of the vectors **b** used in the spatial operator 6.

As the fourth-order dispersion results are clearly less anisotropic than the second-order results, it is interesting to ask how the results behave for a very large order. High-order schemes are often used in reverse-time migration when the model is smooth. Fornberg (1990) has shown that in the limit $M \to \infty$, the standard operator coefficients, c_{mM}, are given by

$$c_{m\infty} = (-1)^{m+1}\frac{4}{\pi(2m-1)^2}, \tag{20}$$

using a limit argument. Equation 20 is also easily derived from the reconstruction formula for bandlimited signals. Provided that $H \le 0.5$ for LEB and $H \le 0.5/\sqrt{3}$ for ROT, this differentiator is exact, and

$$E^{\mathrm{LEB}}(\gamma, H, \hat{\mathbf{k}}) = E^{\mathrm{ROT}}(\gamma, H, \hat{\mathbf{k}}) = \frac{\sin^{-1}(\pi\gamma H)}{\pi\gamma H} - 1. \tag{21}$$

Thus the dispersion error is isotropic in the limit. This is not surprising because only temporal dispersion remains. Even for low order, the ratio given by expression 19 does not differ significantly from $\sqrt{3}$ in three dimensions.

LEB uses four times as much memory per grid cell as the ROT, so the magic number for the ratio $H^{\mathrm{LEB}}/H^{\mathrm{ROT}}$, above which LEB becomes more memory efficient than ROT is $\sqrt[3]{4} = 1.587$. Thus the ROT requires about 20% more memory for the field data for comparable dispersion as $\left(\sqrt[3]{4}/\sqrt{3}\right)^3 = 0.77$. If one set of model parameters — density and 21 stiffnesses — is stored per grid cell the memory advantage of LEB increases dramatically. However, this is not an entirely fair comparison, as there are a number of options for storing the model as mentioned above.

For the same grid spacing the ROT scheme allows a larger time step, but this is almost exactly canceled out by the smaller grid spacing that is required to produce a comparable dispersion. Both the FLOP count and the number of memory accesses per time step are more than twice as high for ROT. The reason is that the calculation of spatial derivatives, in particular stress derivatives, is more costly and involves more data. Four diagonal derivatives, which cannot be reused to calculate other derivatives, must be evaluated for a single stress derivative such as $\partial_x\sigma_{xx}$. Four diagonal derivatives, where each can be reused once for another derivative, must be evaluated for a single off-diagonal stress derivative. Note that for an operator of length $2M$ the LEB stencil for a velocity node contains $18M$ grid elements, whereas the ROT stencil has $24M$, but for stress nodes the corresponding numbers are $18M$ and $48M$, respectively.

An interesting property of the Lebedev grid is that for isotropic models, it decouples into four completely independent Virieux schemes (Davydycheva et al., 2003). It is not hard to show this. A Virieux scheme for the isotropic equation has six stress and three velocity components per grid cell. In the Lebedev cell, we can place the first of these components at four different locations. However, once the first component has been placed the finite difference discretization of equation 2 (the equation of motion) determines the location of the remaining components. Equation 3 (the constitutive equation) doesn't provide new dependencies in the isotropic case.

For a monoclinic material with a plane of symmetry perpendicular to a coordinate axis, the constitutive equation does provide an additional dependency, which joins two Virieux schemes. For such a material the Lebedev grid decouples into two independent schemes with 18 field variables in each. There are three such configurations, one for each of the three symmetry planes. A TTI material with the axis of symmetry in one of these planes has the required symmetry. This means that an inhomogeneous TTI model with the axis of symmetry restricted to vary in, say, the xz plane can be discretized using a scheme with 18 rather than 36 field variables per grid cell, effectively halving the cost both in terms of memory and compute time.

CONCLUSIONS

In this paper we have analyzed and compared the computational requirements and dispersion relationships for the Lebedev and rotated staggered grids for anisotropic, elastic, finite-difference calculations. Comparing the computational costs of these two methods for equivalent dispersion errors, we conclude that the

Lebedev grid is to be preferred. It has the added advantages that it is more straightforward to program and for models with common symmetries, can be decomposed into uncoupled subgrids, and only one of these grids needs to be stored. Therefore, of the two grids proposed, the Lebedev staggered grid is the optimal choice for applications such as reverse-time migration and full-waveform inversion when anisotropy exists. In isotropic media, the Lebedev grid decouples into four Virieux grids, and the Virieux grid is optimal.

The result depends on the fact that $\sqrt[3]{4} < \sqrt{3}$. The first number is the ratio of cell sizes for which the memory requirements for the field variables in the LEB and ROT grids are equal, whereas the second number is the ratio for which the average dispersion is equal. Thus the results can be summarized as follows:

(field variables per cell)$^{\mathrm{LEB}} \approx 4 \times$ (field variables per cel)$^{\mathrm{ROT}}$,

(field variables per vol.)$^{\mathrm{LEB}} \approx (4/3^{3/2}) \times$ (field variables per vol.)$^{\mathrm{ROT}}$,

(CPU cycles per cell)$^{\mathrm{LEB}} \approx 2 \times$ (CPU cycles per cell)$^{\mathrm{ROT}}$,

(CPU cycles per vol.)$^{\mathrm{LEB}} \approx (2/3^{3/2}) \times$ (CPU cycles per vol.)$^{\mathrm{ROT}}$,

where the constant $4/3^{3/2} = 0.77$ represents a saving of 23% in memory, and $2/3^{3/2} = 0.38$, 62% in CPU cycles for LEB over ROT schemes.

The results of the comparison of LEB and ROT in Lisitsa and Vishnevskiy (2010) are compatible with ours.

APPENDIX A

DISPERSIONS RELATIONS

In this appendix, we derive the dispersion relations 11 used for the calculations in this paper. The analysis of the numerical schemes is based on harmonic plane-wave trial functions of type defined in equation 4. A difference operator, D_T, that approximates ∂_t acts on u through multiplication by a function that depends on ω

$$D_T u = f_T(\omega) u. \tag{A-1}$$

Similarly, a difference operator, D_n, that approximates a spatial partial derivative, ∂_n, acts on u through multiplication by function that depends on $\mathbf{k}$

$$D_n u = f_n(\mathbf{k}) u. \tag{A-2}$$

We shall consider a trial vector function of the form

$$v_i = \alpha_i u \tag{A-3}$$

$$\sigma_{ij} = \beta_{ij} u, \tag{A-4}$$

where α_i and β_{ij} are constants (for a plane wave). Substituting equations A-1, A-2, A-3, and A-4 into equations 2 and 3 (the elastic wave equation), we obtain

$$\rho \alpha_i f_T = \beta_{ij} f_j \tag{A-5}$$

$$\beta_{ij} f_T = c_{ijk\ell} \alpha_k f_\ell. \tag{A-6}$$

We eliminate β_{ij} between equations A-5 and A-6 to obtain

$$\rho \alpha_i f_T^2 = c_{ijk\ell} f_j f_\ell \alpha_k. \tag{A-7}$$

Defining

$$p_i = f_i / f_T, \tag{A-8}$$

equation A-7 becomes

$$\alpha_i = c_{ijk\ell} p_j p_\ell \alpha_k / \rho. \tag{A-9}$$

The 3×3 matrix Γ defined by

$$\Gamma_{ik} = c_{ijk\ell} p_j p_\ell / \rho \tag{A-10}$$

is known as the Christoffel matrix. Equation A-9 is a general dispersion relation valid in the homogeneous anisotropic case. It states that the harmonic plane-wave vector trial function only solves the finite-difference equation if an eigenvalue of the Christoffel matrix is unity. For an isotropic material with P-wave velocity α and S-wave velocity β, p_j is a solution if and only if

$$p_1^2 + p_2^2 + p_3^2 = \frac{1}{v^2}, \tag{A-11}$$

where v equals either α or β.

What remains is to derive expressions for the functions f_T and f_i for both the Lebedev and the rotated staggered grids and substitute these in the general isotropic dispersion relation A-11, thus producing the specific dispersion relations we seek. It is easy to verify that for the temporal operator, D_T, defined in equation 5, we have

$$f_T(\omega) = \frac{2\mathrm{i}}{\Delta t} \sin(\omega \Delta t / 2). \tag{A-12}$$

D_S, defined in equation 6, acts on plane-wave trial function through multiplication by the function

$$f_S(\mathbf{k}) = -2\mathrm{i} \left(\sum_{m=1}^{M} c_{mM} \sin((2m-1)\mathbf{k} \times \mathbf{b}) \right). \tag{A-13}$$

D_n^{LEB}, the approximation to ∂_n for LEB, is simply D_S/h with $\mathbf{b} = \hat{\mathbf{e}}_n h/2$, where h is the grid spacing. This means that

$$f_n^{\mathrm{LEB}}(\mathbf{k}) = -\frac{2\mathrm{i}}{h} \left(\sum_{m=1}^{M} c_{mM} \sin\left((2m-1) \frac{hk_n}{2} \right) \right). \tag{A-14}$$

Combining equations A-11, A-12, and A-14 gives the dispersion relation for the LEB scheme:

$$\sin^2\left(\frac{\omega \Delta t}{2}\right) = \left(\frac{v \Delta t}{h}\right)^2 \sum_{n=1}^{3} \left(\sum_{m=1}^{M} c_{mM} \sin\left((2m-1) \frac{hk_n}{2} \right) \right)^2. \tag{A-15}$$

The derivation of an expression for f_n^{ROT} is more longwinded. Let us define the four diagonal vectors:

$$\begin{aligned} \mathbf{d}_0 &= \hat{\mathbf{e}}_1 + \hat{\mathbf{e}}_2 + \hat{\mathbf{e}}_3 \\ \mathbf{d}_1 &= -\hat{\mathbf{e}}_1 + \hat{\mathbf{e}}_2 + \hat{\mathbf{e}}_3 \\ \mathbf{d}_2 &= \hat{\mathbf{e}}_1 - \hat{\mathbf{e}}_2 + \hat{\mathbf{e}}_3 \\ \mathbf{d}_3 &= \hat{\mathbf{e}}_1 + \hat{\mathbf{e}}_2 - \hat{\mathbf{e}}_3. \end{aligned} \tag{A-16}$$

ROT uses the following difference operator to approximate ∂_n:

$$D_n^{\mathrm{ROT}} = \frac{1}{4h} \sum_{j=0}^{3} d_{jn} D_S\left(\frac{h}{2} \mathbf{d}_j\right), \tag{A-17}$$

where d_{jn} is the n-th coordinate of $\mathbf{d}_j$. This means that

$$f_n^{\mathrm{ROT}}(\mathbf{k}) = -\frac{\mathrm{i}}{2h} \left(\sum_{m=1}^{M} c_{mM} \sum_{j=0}^{3} d_{jn} \sin\left(\frac{(2m-1)h\mathbf{k} \cdot \mathbf{d}_j}{2} \right) \right). \tag{A-18}$$

The innermost sum in this expression can be simplified considerably by repeated use of the identity

$$\sin(a+b+c)+\sin(a+b-c)+\sin(a-b+c) + \sin(a-b-c)=4\,\sin(a)\cos(b)\cos(c). \quad \text{(A-19)}$$

Equation A-18 reduces to

$$f_n^{\mathrm{ROT}}(\mathbf{k}) = -\frac{2\mathrm{i}}{h}\left(\sum_{m=1}^{M} c_{mM}\Phi_n^{\mathrm{ROT}}\left(\frac{(2m-1)h\mathbf{k}}{2}\right)\right), \quad \text{(A-20)}$$

where Φ_n^{ROT} is defined in equation 13. From this we obtain the dispersion relation

$$\sin^2\left(\frac{\omega\Delta t}{2}\right) = \left(\frac{v\Delta t}{h}\right)^2 \sum_{n=1}^{3}\left(\sum_{m=1}^{M} c_{mM}\Phi_n^{\mathrm{ROT}}\left((2m-1)\frac{h\mathbf{k}}{2}\right)\right)^2. \quad \text{(A-21)}$$

If we replace Φ_n^{ROT} with Φ_n^{LEB} defined in equation 12, the result is the LEB dispersion relation A-15.

REFERENCES

Anné, L., Q. H. Tran, and W. W. Symes, 1997, Dispersion and cost analysis of some finite difference schemes in one-parameter acoustic wave modeling: Computational Geosciences, **1**, no. 1, 1–33, doi:10.1023/A:1011576309523.

Davydycheva, S., V. Druskin, and T. Habashy, 2003, An efficient finite-difference scheme for electromagnetic logging in 3D anisotropic inhomogeneous media: Geophysics, **68**, 1525–1536, doi:10.1190/1.1620626.

Fornberg, B., 1990, High-order finite differences and the pseudospectral method on staggered grids: SIAM Journal on Numerical Analysis, **27**, no. 4, 904–918, doi:10.1137/0727052.

Holberg, O., 1987, Computational aspects of the choice of operator and sampling interval for numerical differentiation in large-scale simulation of wave phenomena: Geophysical Prospecting, **35**, no. 6, 629–655, doi:10.1111/j.1365-2478.1987.tb00841.x.

Igel, J., P., Mora, and B., Riollet, 1995, Anisotropic wave propagation through finite difference grids: Geophysics, **60**, 1203–1216, doi:10.1190/1.1443849.

Lebedev, V. I., 1964, Difference analogues of orthogonal decompositions, basic differential operators and some boundary problems of mathematical physics I: USSR Computational Mathematics and Mathematical Physics, **4**, no. 3, 69–92.

Lisitsa, V., and D., Vishnevskiy, 2010, Lebedev scheme for the numerical simulation of wave propagation in 3d anisotropic elasticity: Geophysical Prospecting, **58**, no. 4, 619–635, doi:10.1111/j.1365-2478.2009.00862.x.

Lisitsa, V. V., 2007, Lebedev schemes for elastic anisotropic problems: Presented at the 69th EAGE Conference & Exhibition, Extended Abstracts.

Moczo, P., J. O. A. Robertsson, and L. Eisner, 2007, The finite-difference time-domain method for modelling of seismic wave propagation, *in* R. S. Wu, V.Maupin, and R. Dmowska, eds., Advances in wave propagation in heterogeneous earth: Elsevier Academic Press, volume **48**, Advances in Geophysics.

Saenger, E., and T. Bohlen, 2004, Finite-difference modeling of viscoelastic and anisotropic wave propagation using the rotated staggered grid: Geophysics, **69**, 583–591, doi:10.1190/1.1707078.

Saenger, E. H., N. Gold, and S. A. Shapiro, 2000, Modeling the propagation of elastic waves using a modified finite-difference grid: Wave Motion, **31**, no. 1, 77–92, doi:10.1016/S0165-2125(99)00023-2

Virieux, J., 1986, P-SV wave propagation in heterogeneous media: velocity-stress finite difference method: Geophysics, **51**, 889–901, doi:10.1190/1.1442147.